Heliyon 9 (2023) e19625

Contents lists available at ScienceDirect

Heliyon

journal homepage: www.cell.com/heliyon

Research article

A hybrid approach for diagnosing diabetic retinopathy from fundus image exploiting deep features

Mohammed Arif Iftakher Mahmood, Nasrin Aktar, Md. Fazlul Kader *

Department of Electrical and Electronic Engineering, University of Chittagong, Chittagong 4331, Bangladesh

ARTICLE INFO

Keywords:
Abnormal lesions detection
Deep learning
Diabetic retinopathy
Fundus image
Image processing
Inception v3

ABSTRACT

One of the major causes of blindness in human beings is the diabetic retinopathy (DR). To prevent blindness, early detection of DR is therefore necessary. In this paper, a hybrid model is proposed for diagnosing DR from fundus images. A combination of morphological image processing and Inception v3 deep learning techniques are exploited to detect DR as well as to classify healthy, mild non-proliferative DR (NPDR), moderate NPDR, severe NPDR, and proliferative DR (PDR). The proposed algorithm was carried out in several steps such as segmentation of blood vessels, localization and removal of optic disc, and macula, abnormal features detection (microaneurysms, hemorrhages, and neovascularization), and classification. Microaneurysms and hemorrhages that appear in the retina are the early signs of DR. In this work, we have detected microaneurysms and hemorrhages by applying dynamic contrast limited adaptive histogram equalization and threshold value on overlapping patched images. An overall accuracy of 96.83% is obtained to classify DR into five different stages. The better performance demonstrates the effectiveness and novelty of the proposed work as compared to the recent reported work.

1. Introduction

1.1. Background

In 2017, approximately 462 million individuals were suffered from diabetes of type 2 category [1]. Diabetic retinopathy (DR) is a long-term complication of diabetes that affects the retina by blocking the tiny blood vessels of the eye. It is one of the common causes of blindness [2]. Over one-third of the diabetic patients have signs of DR and further one-third of DR is sight-threatening [3]. This has a far reaching economic impact, especially in the 3rd world countries. An affordable and easy early diagnostic system can reduce the risk of blindness caused by DR. DR patients can be classified into five stages: (i) normal/healthy, (ii) mild non-proliferative DR (NPDR) (iii) moderate NPDR (iv) severe NPDR and (v) proliferative DR (PDR). Stage (ii), (iii), and (iv) are called non-proliferative stages with signs of exudates, hemorrhages (HEMs), microaneurysms (MAs), cotton wool etc. as shown in Fig. 1. If left untreated, NPDR may turn into proliferative DR in which new blood vessels called neovascularization (NV) start to grow. Due to improper development, these blood vessels leak easily and affect the vision of a person [4]. To reduce the risk of blindness, early diagnosis is necessary and mass screening of diabetic patients is highly recommended. The diagnosis of DR is processed manually by the ophthalmologists which often gives the correct results but it requires a good knowledge and experience. An automatic screening tool can help the ophthalmologists to detect and analyze DR as well as its stages.

* Corresponding author.
E-mail addresses: arif.im@cu.ac.bd (M.A.I. Mahmood), aktarnasrin33@gmail.com (N. Aktar), f.kader@cu.ac.bd (M.F. Kader).

https://doi.org/10.1016/j.heliyon.2023.e19625
Received 20 January 2023; Received in revised form 28 August 2023; Accepted 29 August 2023

Available online 4 September 2023

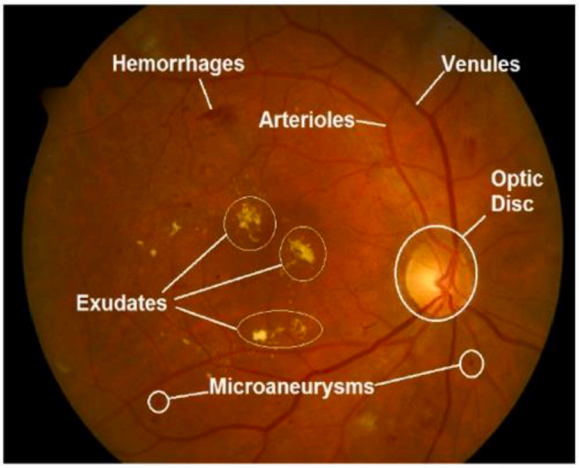

Fig. 1. Retinal image of a DR patient. Different anomalies are indicated [4].

1.2. Related works

Automatic detection of DR based on digital fundus images have been investigated in the literature by exploiting different approaches such as traditional machine learning [5–10] and deep learning [11–16]. A two-level hierarchical architecture to detect MAs was proposed in [5] by exploiting dynamic thresholding and multi-scale correlation filtering. In the first level, candidate MAs were detected using multi-scale correlation filtering, whereas true MAs were classified in the second level by extracting 31 features from the first level candidates. U. Rajendra Acharya et al. [6] proposed a system to identify four different classes of DR such as normal retina, NPDR, PDR, and macular edema. From the 238 retinal fundus images, different texture features were extracted. For automatic classification, these features were fed into the SVM classifier and an overall accuracy of 85.20% was found. To differentiate DR images from the normal, an automatic detection system based on bag of words approach with SVM was proposed in [7]. Speeded up robust features from 180 retinal fundus images were used and an accuracy of 94.40% was obtained. It should be mentioned that the images were collected from the different publicly available datasets.

Mohamed Chetoui et al. [8] reported a DR detection method using different texture features such as local energy-based shape histogram (LESH) and local ternary pattern. From the experimental results, it was observed that LESH outperformed the others to differentiate between DR and non-DR. An accuracy of 90.40% was obtained using SVM with a radial basis function kernel. Nasr Gharaibeh et al. [9] designed an automated system to detect DR composing of several steps such as pre-processing, different anomalies detection and removal, feature extraction, feature selection, and classification. Using DIARETDB1 dataset and SVM with genetic algorithm as a classifier, an accuracy of 98.40% was obtained. Adrian Colomer et al. [10] extracted textural and morphological information by computing local binary patterns and granulometric profiles in fundus images to detect the early signs of DR. The extracted information were then fed to the classifiers. The performance was studied in terms of three different classifiers such as SVM, random forest, and Gaussian processes.

Deep learning (DL) algorithm is considered as an effective and advanced form of machine learning, has gained momentum in recent years. Researchers have been trying to utilize deep learning for medical image analysis. To identify the different stages of DR, a convolutional neural network (CNN) based deep learning approach was investigated in [11]. It was reported that misclassification of the mild disease as normal can be occurred owing to the inability of the CNN model to identify the subtle features of DR. Therefore, to improve the detection accuracy, contrast limited adaptive histogram equalization (CLAHE) was applied before training the DR images. The experimental results demonstrated 57.20%, 68.80%, and 74.50% accuracies for 4-ary, 3-ary, and 2-ary classification models, respectively. To identify the different stages of DR, a CNN based model was presented in [12]. Based on the severity of DR, images were categorized into five different grades, where lowest grade (i.e., 0) represented normal/healthy and highest grade (i.e., 4) represented PDR. Yung-Hui Li et al. [14] proposed an algorithm based on deep CNN, SVM, fractional max pooling, and teaching-learning based optimization to classify DR into five different stages. The method was evaluated using the online public Kaggle dataset and an average accuracy 86.17% was obtained. The authors also designed an app named “Deep Retina” for the easy screening system.

In [13,15], the authors designed two-step DCNN algorithm to detect the small lesion and MAs. In the first step, MAs are detected and the final step was used to reduce the number of false positive in the detection process. Note that the number of false positive was more than 6 per image in the final result. A hybrid DR detection method by using image processing and deep learning was presented in [16]. Both CLAHE and histogram equalization (HE) were employed and the classification performance was evaluated by CNN. To validate the proposed method, 400 retinal images from Messidor dataset were used and 97% accuracy was reported. For segmenting DR lesions, a Bayesian approach was proposed in [17]. The method was evaluated on IDRiD dataset. The experimental results demonstrated area under precision-recall curve 0.641 for soft exudates, of 0.84 for hard exudates, 0.484 for MAs, and 0.593

for HEMs. A hybrid neural network approach was investigated in [18] for DR detection. The model was evaluated on different public datasets. Furthermore, existing deep learning based DR detection techniques were surveyed in [19,20].

To design an alternative and hybrid method for diagnosing DR from fundus images is the main objective of this study. Our motivation is to improve the classification result by using image processing and deep learning. We have detected MAs and HEMs using image processing and NV using deep learning. This approach applies dynamic CLAHE and thresholding level for intensity-based detection and localization of MAs and HEMs in retinal images. There exist contrast and brightness variations in the original fundus images. So, in this case, global thresholding level can not be used. We have used Isodata thresholding to find automatic threshold value for a given gray image. To reduce the number of false positives in our approach, we have removed blood vessels, macula, and optic disc from the processed image. Based on the presence of MAs, HEMs, and NV, the image is classified as normal/healthy, different NPDR stages (e.g., mild, moderate, and severe), and PDR. Throughout this study, our aim is to provide an effective solution to classify early stage DR for clinical benefits. Though detection of MAs and HEMs is not new, but in our proposed method, we have used a novel patching algorithm along with image processing tweaks and found better overall accuracy than previously reported works.

1.3. Contributions

The major contributions of this study are summarized as follows.

- A hybrid model is proposed, where a combination of morphological image processing and Inception v3 deep learning techniques are exploited to detect DR, where DR can be classified as normal/healthy, NPDR (e.g., mild, moderate, and severe), and PDR.
- Compared to the recent reported works, the proposed scheme shows improved performance. An overall accuracy of 96.83% is obtained to classify DR into five stages.
- The proposed model automatically detects DR from any retinal image, where any expert supervision is not required.

1.4. Paper organization

The remainder of this paper is organized as follows. Section 2 describes the methodology of the system in detail. Section 3 presents the result of the proposed model. A comparative study with the other reported works is also discussed in this section. Finally, the conclusion of this paper is drawn in Section 4.

2. Methodology

Before detecting MAs and HEMs, it is important to remove the large features such as optic disc, macula, and the blood vessels. So, the following tasks were done: segmentation of blood vessels, localization of macula and optic disc, MAs, HEMs detection, and classification of NV. We have detected blood vessels, macula, optic disc, MAs and HEMs using python in OpenCV platform and NV using deep learning. Inception v3 classifier was used as a deep learning algorithm. We have designed a web server that can detect DR. The web is designed such that one can post a retinal image to the server and can get the results in return. The overall architecture is depicted in Fig. 2.

2.1. Segmentation of blood vessels

To prevent false positives, it is necessary to remove the blood vessels from the retinal image before applying MAs/HEMs detection algorithms. Different filtering approaches were previously reported such as filling algorithm and multi-directional top hat transformation [21], Gabor, Frangi and Gauss filters [22], Hessian multiscale enhancement filter [23], reconstruction and top hat transformation [24] etc. Adaptive histogram equalization was used in this work for the enhancement of retinal image. Our proposed method is depicted in Fig. 3.

To extract the blood vessels, the image was first resized to 500×500 pixels as shown in Fig. 4(a). This reduced calculation time without any performance degradation. Only green channel was used due to superior contrast and better noise performance. In the next step, CLAHE was applied to increase the contrast of the image as in Fig. 4(b). To remove background, we blurred the contrasted image using averaging filter and subtracted that from the contrast enhanced image as shown in Fig. 4(c). After reapplying CLAHE, the images were converted into binary using threshold levels of individual images computed using Isodata method.

Isodata technique is a method that can calculate threshold value automatically from a grayscale image. Firstly, it calculates gray values of all pixels using histogram analysis. We used 256 bins for the range of 0 to 255. Then, mean threshold value was calculated by taking the mean of all the gray values. All the pixels were divided into two groups based on the mean threshold value. From these two groups, we have calculated two average intensity values. One is below than mean threshold value and termed as MBT, whereas the another one is above than mean threshold value and termed as MAT. These two values were calculated by taking the average of the gray values. The threshold value is then found by taking the average of MBT and MAT as in Equation (1).

$$T_h = \frac{\mathrm{MBT} + \mathrm{MAT}}{2}. \tag{1}$$

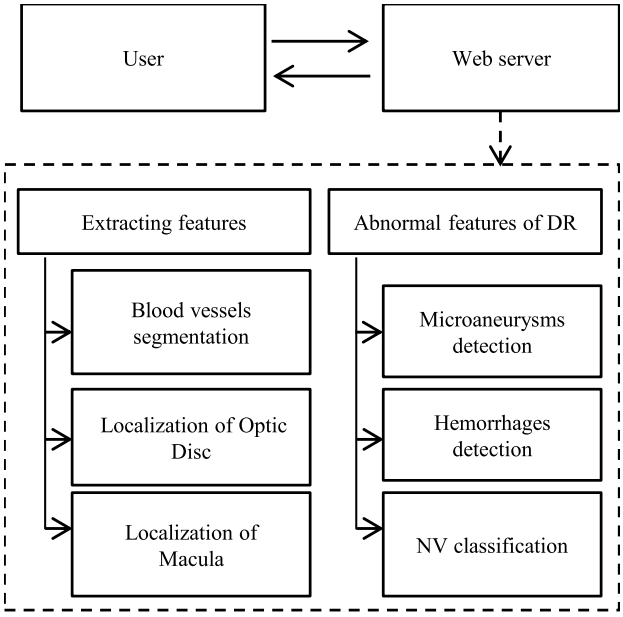

Fig. 2. Proposed architecture of the system. It is composed of cloud block (image processing and deep learning algorithm on cloud computing platform) and user block.

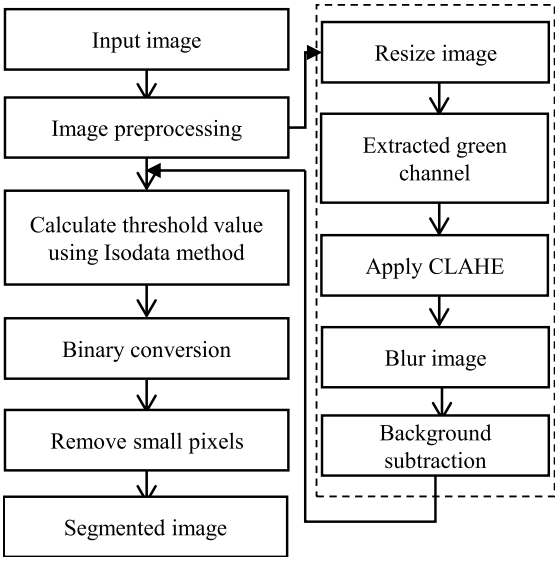

Fig. 3. Framework for segmentation of blood vessels.

Until the convergence is obtained, the new threshold value is iteratively updated by the new average intensity values. In each iteration, as the threshold value T_h changes, MBT and MAT values are recalculated based on the updated threshold value. Note that Isodata is a well-known technique to find a threshold value and widely used in the literature.

Once we get the binary image as in Fig. 4(d), we have to perform some post processing steps to enhance the performance of the algorithm. Falsely detected small blood vessels were removed by using an area limiting threshold. In a binary image of a DR patient, large HEMs were detected along with blood vessels. To remove them, we calculated contour area, perimeter, and approximated contour shapes. The shape approximation was used to differentiate between blood vessels and HEMs. Finally, morphological opening and closing were applied to extract blood vessels as shown in Fig. 4(e).

2.2. Localization and removal of optic disc

Optic disc localization and removal from the retinal image is necessary for the detection of DR features. Different optic disc localization algorithms such as local feature spectrum analysis [25], entropy calculation [26], bat meta-heuristic algorithm [27],

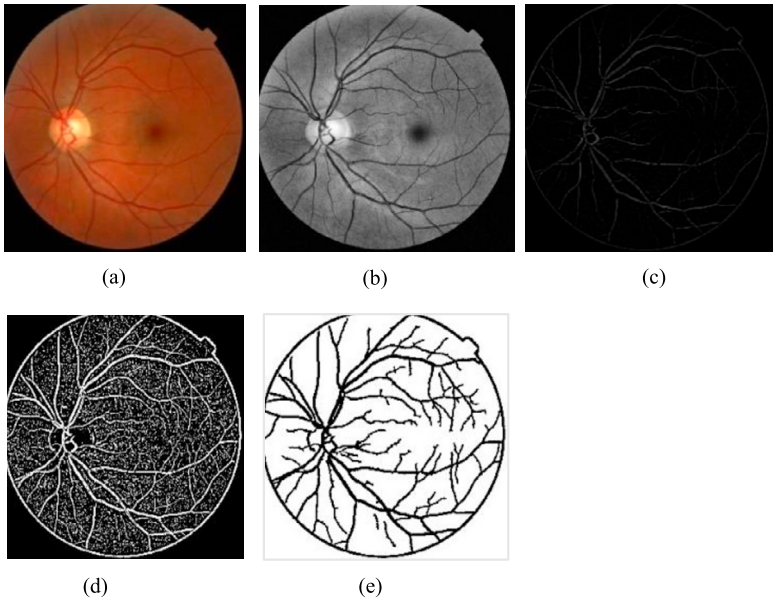

Fig. 4. Segmentation of blood vessels (a) Input image, (b) Green channel after applying CLAHE, (c) After subtraction from the blurred image, (d) Binary image, (e) Final image by removing unwanted pixels.

statistical edge detection and circular Hough transformation [28], structured learning [29] etc. have been suggested before. Recently, few researchers have worked on deep learning to localize optic disc [30–32]. Optic disc differs in size, appearance, and location in the original retinal images. Human can recognize these features easily due to its characteristics but it is difficult to localize automatically by the above proposed algorithms. Here, we propose a modified image processing method that can localize optic disc very precisely as described below.

We visualized that optic disc is the brightest spot of the retinal images. We used the brightest spot detection algorithm using a OpenCV function called minMaxLoc(). As the exudates and cotton wools have the same or more intensity than optic disc, this algorithm detected those spots as optic disc on abnormal images. To solve that problem, we changed the color space from BGR to HSV format as HSV color space highlights the optic disc much better than the LAB or LUV format. Later we applied CLAHE on every channel of input image and converted the image to the grayscale. Note that the different stages of optical disc localization is shown in Fig. 5(a)–5(e). The CLAHE function is extremely susceptible to noise. To remove that noise, we used image blurring Gaussian filter conducted from a linear operation as Equation (2).

$$G(x, y, \sigma) = \frac{1}{2\pi\sigma^2} e^{-\frac{x^2+y^2}{2\sigma^2}}, \tag{2}$$

where, the level of blurring of the image depends on σ. To find the brightest spot of the image, we utilized an OpenCV library function and later drew a circle around the region as shown in Fig. 5(d).

2.3. Localization and removal of macula

Macula is in charge of central vision. However, its presence in the output image leads to the false detection of MAs and HEMs. To remove this, at first we resized the image into 2000×1800 pixels and removed the black background of the image. Then, CLAHE was applied on every channel of the image after converting it to LAB format. The processed image was then blurred using bilateral filter. Tomasi and Manduchi proposed the design of the bilateral filter which is a non-linear filter and it is used to smoothen images [33]. Note that the framework for localization of macula is shown in Fig. 6 and the different stages of macula detection is shown in Fig. 7(a)–7(e). Different linear filters such as Gaussian filter and mean filter often tend to lose important edge information since they blur out everything. To solve that problem, the non-linear bilateral filter was introduced. But the operation of this filter is slower than other filters. The bilateral filter (BF) is demonstrated in Equation (3) [34].

$$BF[I]_p = \frac{1}{W_p} \sum_{qoS} G_{\sigma_s}(||p-q||) G_{\sigma_r}(|I_p - I_q|) I_q, \tag{3}$$

where, W_p is the normalization factor, σ_s denotes the size of the neighborhood and σ_r controls the sharp of the edge. The filtered image was then converted to gray scale image before binarization. Finally, the binary image after removing noise is found as shown in Fig. 7(e).

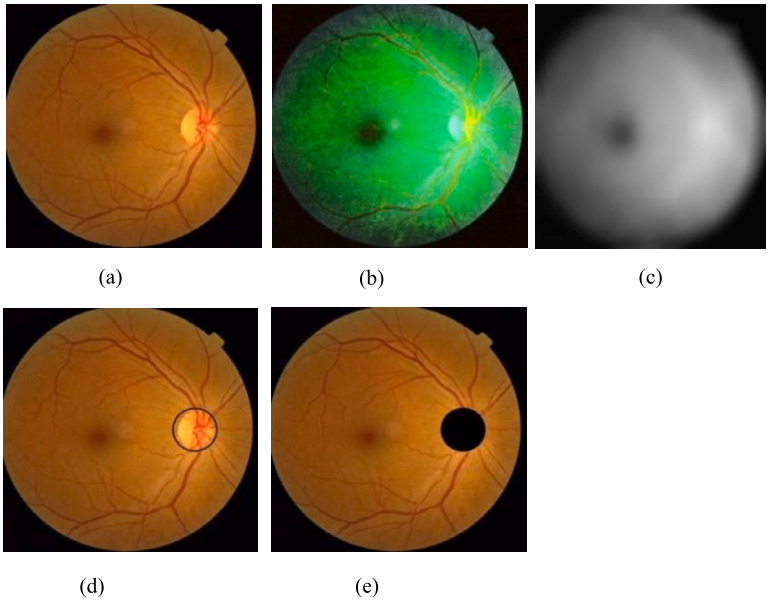

Fig. 5. Optic disc localization: (a) Input image, (b) After applying CLAHE on HSV format, (c) Gray image after blurred, (d) Draw a circle, (e) Final image (removal of optic disc).

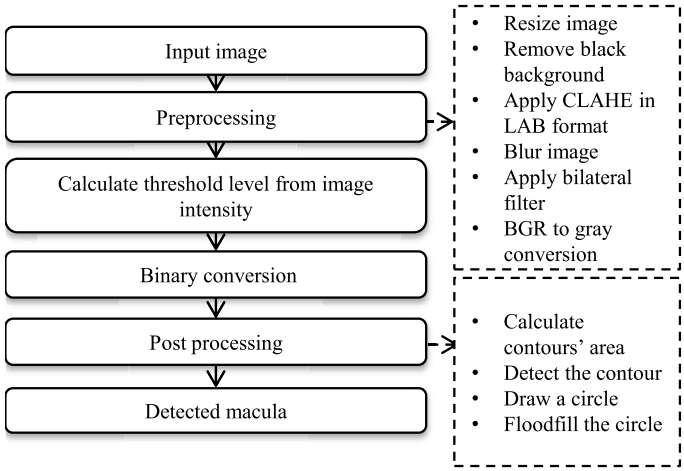

Fig. 6. Framework for localization of macula.

2.4. Microaneurysms detection

Microaneurysms are the first sign of diabetic retinopathy and therefore the detection of these lesions are very important for classifying whether the patient has any sign of DR or not. But the size of the MAs is in micrometer range. So, it is difficult to manually inspect these in fundus image. An automatic screening tool to detect these lesions can help the ophthalmologists for the grading of diabetic retinopathy. Numerous research works in this area have been reported [5,13,15]. We have used a modified technique as depicted in Fig. 8 to detect MAs, where each image was segmented into 100×100 pixels. We have overlapped 15×15 pixels by analyzing images. After applying CLAHE on those patches, we converted them into binary images using Isodata technique to determine an appropriate threshold value. Subsequently, blood vessels, HEMs, and macula were removed from the binary patches and then MAs were extracted by calculating contours' area. Noise generated due to contrast enhancement was removed by using 2D convolution filter which is accomplished by doing a convolution between a kernel and an image. The general expression of convolution is depicted in Equation (4).

$$g(x,y) = w * f(x,y) = \sum_{dx=-a}^{a} \sum_{dy=-b}^{b} w(dx,dy) f(x+dx, y+dy) \tag{4}$$

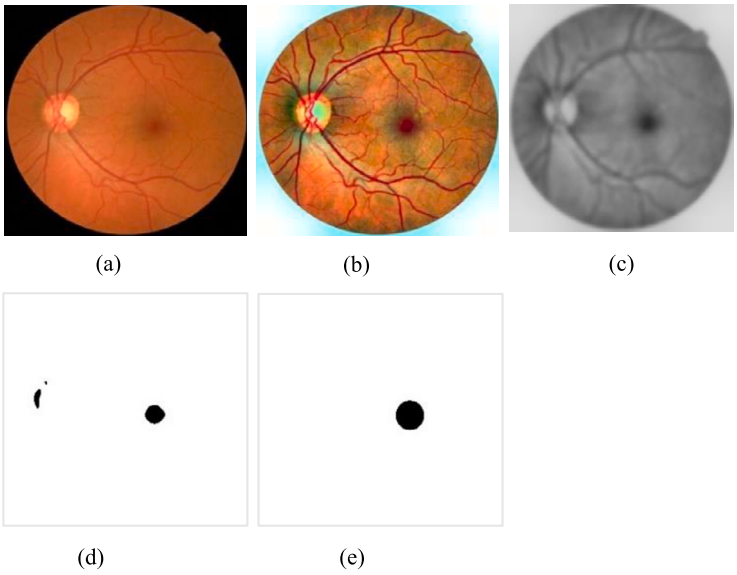

Fig. 7. Macula detection (a) Input image, (b) After applying CLAHE, (c) Gray image after applying filter, (d) Binary image, (e) Final binary image after removing noise.

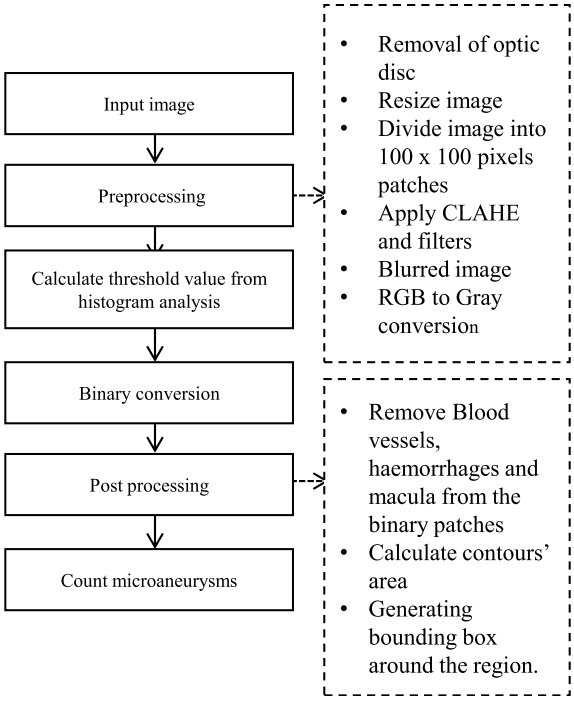

Fig. 8. Framework for detection of microaneurysms.

where, $f(x, y)$ is the original image, $g(x, y)$ is the filtered image, and w is the filter kernel. Note that the different stages of microaneurysms detection is shown in Fig. 9(a)–9(e).

2.5. Hemorrhages detection

Counting HEMs is important to classify moderate NPDR, severe NPDR, and PDR images. We divided each image into 25 overlapping patches and then processed to detect them. We have overlapped by 100×100 pixels. Dividing into patches reduce the false positives to almost zero which was rather difficult to automate when trying with the whole image. We have detected HEMs by

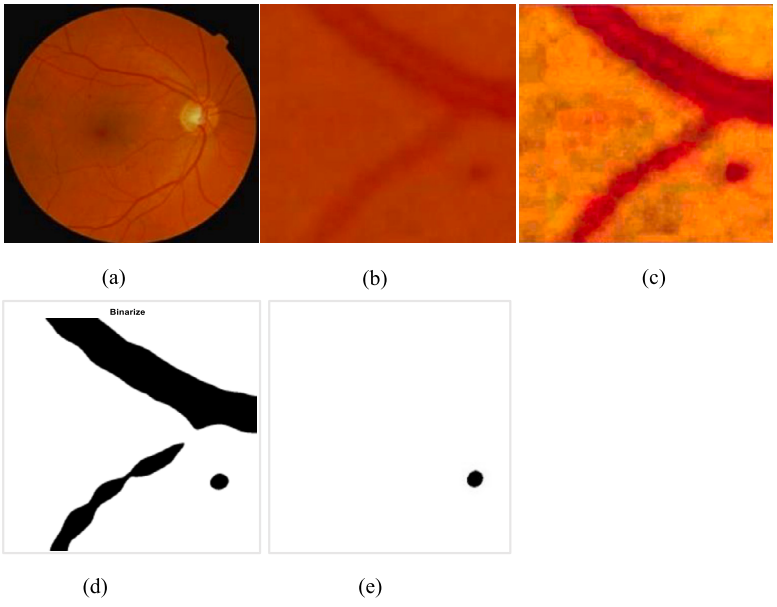

Fig. 9. Microaneurysms detection (a) Original image, (b) Patch of the image, (c) After applying CLAHE, (d) Binary image, (e) Removed blood vessels from the binary image.

dividing images in smaller blocks instead of whole image due to its advantage. Some of the advantages of our patch-based method are:

- Since image is breaking down into smaller patches, we can analyze its detailed local features and their relationship which is effective in finding any abnormalities present in the image.
- In digital image, there exist contrast and brightness variation in image. For that, globally assigned variables of any parameter such as CLAHE, global threshold does not work better. Our patch-based approach reduces this global inconsistent effect since it has to work on smaller patches, where there is minimal room for variation. Thus, false positive is reduced in our proposed method.

Like MAs detection, the HEMs were also detected by dividing image into multiple patches and subtracting blood vessels and macula from the binary image. The differences between these two algorithms were the number of patches, the threshold level and other parameters of the functions. The other parameters are contours area, clip limit, and tiles grid size of CLAHE. The efficiency of CLAHE depends on the clip limit and tiles grid size [35]. After image processing, the contours were detected and the number of present HEMs in the input image were counted. The different stages of HEMs detection is shown in Fig. 10(a)–10(e).

Although the mechanisms of MAs and HEMs detections were same, two different algorithms were used. At the time of removing large blobs from the segmented blood vessels, few small blood vessels were also removed. This increased the number of false positives at the detection time of MAs. But the removal of those small blood vessels did not create issue at the detection of HEMs as the size of patches in the HEMs detection was greater than the MAs ones.

2.6. Neovascularization classification

PDR is characterized by the growth of new abnormal blood vessels called NV on the surface of the retina or optic nerve. Different NV detection algorithms such as multivariate m-Mediods based classifier [36], mutual information maximization [37], extreme learning machine [38], and feature extraction [39] have been reported to isolate abnormal blood vessels from fundus image. These works were based on hand-crafted feature extraction and classification to detect NV. These systems are highly sensitive to the quality of images.

Among various deep learning architectures such as AlexNet, VGGNet, ResNet, GoogLeNet, Inception v2, and Inception v3, top-1 and top-5 errors are lower for inception v3 classifier which is evaluated on ImageNet dataset [40]. Another advantage of Inception v3 is that multiple kernels of different sizes can be implemented in the same layers depending on the features of an image. Hence, we have used tensorflow inception v3 classifier to classify whether there is any presence of NV or not. The first step before training the neural network is to collect enough retinal images. These images were used as a reference for the classifier. The training images contained good variations. The performance of inception v3 classifier depends on the number of training data. But the number of PDR images available for our training was limited as we were constrained to use a small fraction of PDR images from Kaggle dataset due to the low quality of the images. For training purposes, we selected patches with NV as positive samples and patches without NV as negative samples. As there existed class imbalance problem, we augmented NV patches to obtain a stable model. For data

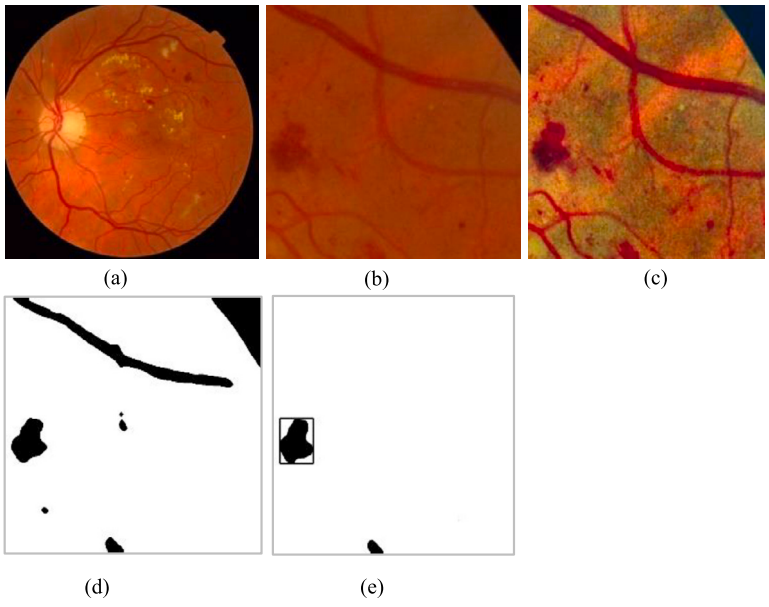

Fig. 10. Hemorrhages detection (a) Input image, (b) Patch of the image, (c) After Applying CLAHE, (d) Binary image, (e) Removed blood vessels and macula from the binary image.

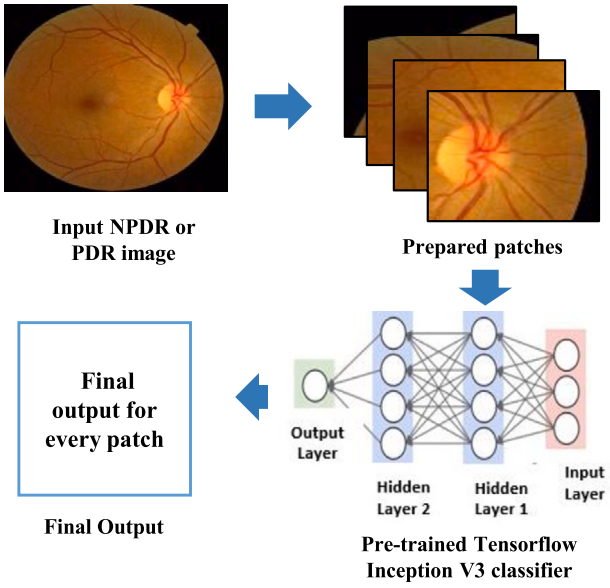

Fig. 11. Steps of the development process of the proposed method.

augmentation, we have rotated and flipped the images in both horizontally and vertically. Thus, sufficient images were obtained and trained our model using 350 non-NV patches and 350 NV patches. For testing purpose, we first divided the images into 4 equal parts and tested every patch using inception v3 default features. If NV is classified in any of the patch, the image is classified as PDR image. The architecture of our proposed algorithm is illustrated in Fig. 11. Note that the parameter settings for the inception v3 are provided in Table 1.

3. Result and discussion

3.1. Dataset

We have used publicly available Drive [41], Messidor [42], Kaggle [43], Stare [44], and DIARETDB0 [45] datasets to evaluate our proposed model. The dataset Drive is used to evaluate and compare algorithms on blood vessel segmentation. The images in Messidor database are classified into four stages by the ophthalmologists based on the number of present MAs and HEMs. We have

Table 1
Parameter settings for the inception v3.

Parameters	Value
Image size	299×299
Number of Class	2
Epochs	100
Learning rate	0.01
Batch size	100

used 437 images from the Messidor dataset to evaluate our DR detection algorithm. Besides that, we have used this database to calculate accuracy of MAs, HEMs, macula and optic disc detection. The Kaggle dataset contains 35,126 graded training images and 53,576 non-graded test color fundus images of different resolutions. It has five categories of DR images. We have used 68 PDR images from the training dataset considering image quality. Moreover, 30 PDR images from Messidor, Stare, and DIARETDB0 datasets are used for the evaluation of the classifier.

3.2. Performance evaluation

We have studied the performance of the proposed model in terms of sensitivity, specificity, and accuracy. In this study, we have applied blood vessels segmentation algorithm on Drive dataset due to the availability of retinal images and the corresponding binary images. We have used the binary images as ground truth to investigate the performance of the proposed model. For that, we have compared our obtained binary images pixel by pixel with provided binary images of the Drive dataset. Secondary metrics such as true negative (TN), true positive (TP), false positive (FP), and false negative (FN) were calculated. Using the manual result as a reference, we obtained 79.13% sensitivity, 96.65% specificity, and an accuracy of 95.14%.

We conducted an assessment using a dataset of 1200 images from Messidor database to evaluate the performance of optic disc localization. Among these images, 13 images manifested false localization of optic disc due to low image brightness. The obtained accuracy is 98.92%, whereas prior to utilizing CLAHE on HSV format, we observed 54 images of falsely localized optic disc, resulting in an accuracy of 95.50%. We computed accuracy by the ratio of correctly localized optic disc to the total number of images. The proposed method for macula localization was evaluated on 1200 images from Messidor dataset. Out of these images, 87 images could not localize macula, resulting in an accuracy of 92.75%.

We have used image processing to detect MAs in DR images instead of utilizing deep learning techniques. As mentioned in [11], errors mainly occur in the misclassification of mild NPDR as normal because CNN models can not detect the subtle features of DR. To grade DR, MAs and HEMs must be counted. But the detection of MAs using two-step deep learning [13,15] did not yield satisfactory result due to the false detection. The number of false positives is more than 6 per image as in [15]. Since we are grading our images based on MAs, this number of false positives will lead to misclassification of fundus images. In our algorithm, the number of false positives is almost zero due to subtraction of other features from processed patches. However, our accuracy is slightly dropped due to the number of false negatives. The main reason is the position of the MAs. If the MAs are situated on the blood vessels or near the blood vessels or macula, our algorithm cannot detect it as it often identifies them to be a part of blood vessel or macula and subtracted with those regions. Another problem is the camera artifacts, dark, blurred, uneven illumination, and low contrast images. Analysis on low quality images produces unreliable results in spite of the presence of MAs; the system labels an image as normal. To evaluate our algorithm, we have used images from Messidor database. But in this database, only the DR stage is mentioned. We have calculated manually the number of present MAs in retinal images and compared with our obtained data. The obtained sensitivity, specificity, and accuracy are 82.21%, 95.34%, and 90.43%, respectively. The detailed experimental settings to simulate the proposed model are summarized in Table 2.

We encountered similar challenge in detecting HEMs as MAs which are the cause of false negatives of our method. In our assessment, we tested 250 images without HEMs and identified 4 images, where the method falsely determining a section of blood vessels as HEM. At the time of removing HEMs from the segmented blood vessels, some of thin blood vessels were also removed which are the reason of false positives. The obtained sensitivity, specificity, and accuracy are 80.70%, 98.4%, and 89.83%, respectively. As mentioned earlier, to test the classifier, we have gathered some PDR images from different databases and tested them. The overall accuracy of our NV classifier was 98.71%.

Execution times for each step are mentioned in Table 3. We used a machine with Windows 10, 64-bit OS, Intel(R) Core (TM) i5-6200U CPU @2.30 GHz, and 8.00 GB RAM. The execution time to detect MAs is 22 seconds. We have detected MAs by dividing the images into overlapping 100×100 pixels. If MAs are situated on the edges of the patches, then algorithm can not calculate those lesions. That is why, overlapping was done. The number of patches in hemorrhages is much lower compared to MAs. As a result, the required time is less than the MAs detection times.

To discuss the overall performance, we have tested 467 images to evaluate our algorithm. Among them, 437 images were from Messidor database, remaining 30 images selected from different databases were PDR images as mentioned earlier. The first stage, which is normal, contributes the greatest number of 220 images. Remaining 247 images are abnormal images. The abnormal or diabetic retinopathy images are classified into NPDR (e.g., mild, moderate, and severe) and PDR.

Based on the ground truth provided by the experts, we have calculated TN, TP, FN, and FP. The values are listed in Table 4. We have calculated accuracy, specificity, and sensitivity for five types of retinal images. The chart is depicted in Fig. 12. As shown in Fig. 12, normal/healthy, NPDR (e.g., mild, moderate, and severe), and PDR are represented as different classes. The overall accuracy

Table 2
Experimental settings.

Title	Parameter name	Blood vessel extraction	Macula detection	Optic disc detection	Microaneurysms detection	Hemorrhages detection
Image dataset	Dataset Name	Drive	Messidor	Messidor	Messidor	Messidor
	Number of Images	20	1200	1200	437	437
	Resolution	565 × 584	2240 × 1488, 1440 × 960, 2304 × 1536	2240 × 1488, 1440 × 960, 2304 × 1536	2240 × 1488, 1440 × 960, 2304 × 1536	2240 × 1488, 1440 × 960, 2304 × 1536
	Image Resize	500 × 500	2000 × 1800	2229 × 2194	–	–
	Image Patch	–	–	–	100 × 100	Image width/25 × image height/25
Image processing	Image Channel	Green				
	Color Space	BGR	LAB	HSV	LAB	LAB
	CLAHE	Clip Limit: 2.0, Tiles Grid Size: (4, 4)	Clip Limit: 4.0, Tiles Grid Size: (4, 4)	Clip Limit: 4.0, Tiles Grid Size: (4, 4)	Clip Limit: 6.0, Tiles Grid Size: (4, 4)	Clip Limit: 4.0, Tiles Grid Size: (4, 4)
	OpenCV Blur	Kernel Size: (70, 70)	Kernel Size: (50, 50)	Kernel Size: (200, 200)	Kernel Size: (20, 20)	Kernel Size: (10, 10)
	Gaussian Blur	–	–	Kernel Size: (5, 5)	–	–
	Filter 2D	–	–	–	Kernel Size: (5, 5)	Kernel Size: (5, 5)
	Bilateral Filter	–	Diameter: 50, Sigma Color: 100, Sigma Space: 100	–	–	–
	Threshold Value	Isodata technique	Mean Intensity of image/6	–	Isodata technique	Isodata technique
	Area Limit	3000	–	–	–	–
	Epsilon of Approximate Shape	0.05 * Perimeter	–	–	–	–
	Morphological Opening	Kernel: (4, 4), Iterations: 3	–	–	–	–
	Position of Macula	–	530 < x axis < 1500, 525 < y axis < 1030	–	–	–
	Contours Area	–	–	–	30 < Area < 850	370 < Area < 30000
Evaluation metrics	Sensitivity	79.13%	–	–	82.21%	80.70%
	Specificity	96.65%	–	–	95.34%	98.4%
	Accuracy	95.14%	92.75%	98.92%	90.43%	89.83%

Table 3
Execution time of the proposed method.

Properties of retina	Execution time
Blood Vessels	1.6 s
Optic Disc	0.32 s
Macula	2 s
Microaneurysms	22 s
Hemorrhages	8 s
Neovascularisation	4 s

Table 4
Parameter metrics of DR classification stages.

Type	TP	FN	TN	FP
Normal	209	11	241	6
Mild NPDR	48	7	400	12
Moderate NPDR	62	8	384	13
Severe NPDR	85	7	371	4
PDR	28	2	433	4

is obtained as 96.83% and calculated by (all TPs + all TNs)/(all TP + all FP + all TN + all FN), where the values of FP, TP, FN, and TN are shown in Table 4.

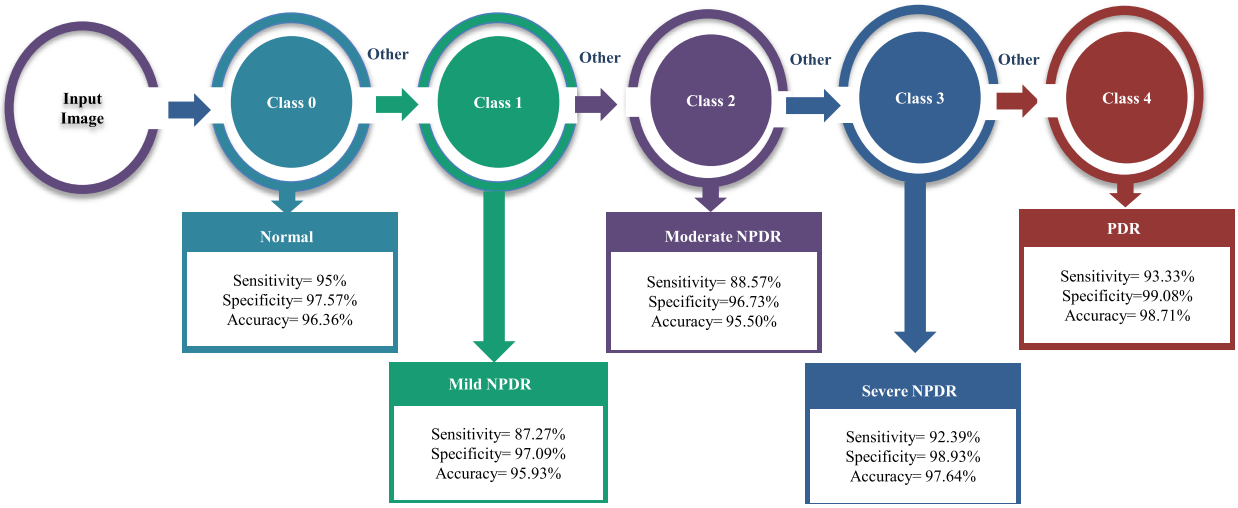

Fig. 12. Classification results of DR stages, where sensitivity, specificity and accuracy are shown.

Table 5
Comparative evaluation of DR vs Non-DR in terms of the sensitivity, specificity, and accuracy.

Methods	Pub. Year	Used Dataset	Classifier	Sensitivity	Specificity	Accuracy
U. Rajendra Acharya et al. [6]	2012	Messidor	SVM	98.5%	89.5%	85.2%
Mohamed Chetoui et al. [8]	2018	Messidor	SVM	–	–	90.4%
Carson Lam et al. [11]	2018	Kaggle and Messidor	CNN	–	–	74.5%
Yung-Hui Li et al. [14]	2019	Kaggle	DCNN+SVM+TLBO	89.30%	90.89%	91.05%
Enrique V. Carrera [46]	2017	Messidor	SVM	94.6%	66.2%	80.4%
Marwan D. Saleh [47]	2012	–	SVM	89.47%	95.65%	–
Proposed Method	–	**Kaggle+Messidor**	**Image processing+DCNN**	**97.57%**	**95%**	**96.36%**

Table 6
Accuracy comparison for different stages of DR.

Methods	Pub. Year	Normal	Mild NPDR	Moderate NPDR	Severe NPDR	PDR
Yung-Hui Li et al. [14]	2019	97.67%	22.09%	72.60%	33.61%	50.50%
Enrique V. Carrera [46]	2017	80.5%	92.5%	83%	84.5%	–
Proposed Method	–	**96.36%**	**95.93%**	**95.50%**	**97.64%**	**98.71%**

3.3. Comparative analysis

We have compared our results with some of the recent works to show the efficacy of the proposed model. The analysis is shown in Table 5 and 6. In Table 6, we have compared our five stages classification results with some recent works. The comparison is based on accuracy (the ability to diagnose correctly), sensitivity (actual positives that are correctly identified as positive), and specificity (actual negatives that are correctly identified as negative). Considering Tables 5 and 6, results can be explained briefly as follows:

- The proposed hybrid method (i.e., image processing and DCNN) provided 97.57% sensitivity, 95% specificity and 96.36% accuracy in terms of DR vs non-DR classification as shown in Table 5.
- But our main focus is to classify DR into five different categories. In terms of accuracy, it is obtained 96.36%, 95.93%, 95.50%, 97.64%, and 98.71% for normal image, mild NPDR, moderate NPDR, severe NPDR, and PDR, respectively.
- It is seen from Tables 5 and 6 that our proposed method provides better result than the reported literature.
- From Table 5, it is found that [6] shows better performance in terms of sensitivity as compared to the proposed method. On the contrary, the proposed method outperforms [6] in terms of specificity. However, the overall accuracy is better in the proposed method.
- Moreover, from Table 5, it is apparent that although [47] shows slightly better performance in terms of specificity, the proposed method outperforms [47] in terms of sensitivity. Note that the performance of [47] was not studied in terms of accuracy.
- The proposed method shows improved performance as compared to the reported literature which is clear from Tables 5 and 6.

The main objective of the proposed method was to classify images into five different stages. The primary stages often have MAs and HEMs. So, it is very crucial to identify those lesions correctly to detect DR which we have accomplished by using patch based and dynamic thresholding method.

4. Conclusion

In this study, we have presented a hybrid approach to diagnose diabetic retinopathy using image processing and deep learning algorithms. We have used image processing to detect five different features such as blood vessel segmentation, macula and optic disc localization, MAs and HEMs detection. The main feature of PDR (i.e., NV) was classified by using tensorflow inception v3 classifier. To study the performance our DR detection algorithm, 437 images from the Messidor dataset were exploited. Moreover, 68 PDR images from the Kaggle's training dataset considering image quality and 30 PDR images from the Messidor, Stare and DIARETDBO were used to evaluate the performance of the classifier. Based on the dataset analysis, the results showed that the proposed model achieved 97.57% sensitivity, 95% specificity, and 96.36% accuracy in terms of DR vs non-DR. In terms of accuracy, 96.36%, 95.93%, 95.50%, 97.64% and 98.71% are obtained for normal, mild NPDR, moderate NPDR, severe NPDR, and PDR, respectively. Moreover, an overall accuracy of 96.83% is achieved in the proposed method to classify DR into different stages. It is apparent that the proposed method shows improved performance as compared to the reported literature by considering different performance metrics. Furthermore, the algorithm is designed such that there is no need of expert supervision. The user only needs to know how to capture the image as the accuracy of the algorithm depends mainly on the input image. However, we expect that with current imaging technology, poor quality images will not be an issue. Thus we hope that the proposed system will be efficiently used as a helping hand to detect DR by the ophthalmologists because of its high level of accuracy.

Funding statement

The authors would like to thank Research and Publication cell, University of Chittagong for their financial support.

CRediT authorship contribution statement

Mohammed Arif Iftakher Mahmood: Conceived and designed the experiments; analyzed and interpreted the data; contributed reagents, materials, analysis tools or data; wrote the paper; **Nasrin Aktar**: Conceived and designed the experiments; performed the experiments; contributed reagents, materials, analysis tools or data; wrote the paper. **Md. Fazlul Kader**: analyzed and interpreted the data; contributed reagents, materials, analysis tools or data; wrote the paper.

Declaration of competing interest

The authors declare that they have no known competing financial interests or personal relationships that could have appeared to influence the work reported in this paper.

Data availability

Data will be made available on request.

Additional information

No additional information is available for this paper.

References

[1] M.A.B. Khan, M.J. Hashim, J.K. King, R.D. Govender, H. Mustafa, J. Al Kaabi, Epidemiology of type 2 diabetes – global burden of disease and forecasted trends, J. Epidemiol. Glob. Health 10 (1) (2020) 107–111, https://doi.org/10.2991/jegh.k.191028.001.

[2] J.L. Leasher, R.R. Bourne, S.R. Flaxman, J.B. Jonas, J. Keeffe, K. Naidoo, K. Pesudovs, H. Price, R.A. White, T.Y. Wong, et al., Global estimates on the number of people blind or visually impaired by diabetic retinopathy: a meta-analysis from 1990 to 2010, Diabetes Care 39 (9) (2016) 1643–1649, https://doi.org/10.2337/dc15-2171.

[3] R. Lee, T.Y. Wong, C. Sabanayagam, Epidemiology of diabetic retinopathy, diabetic macular edema and related vision loss, Eye Vis. 2 (1) (2015) 1–25, https://doi.org/10.1186/s40662-015-0026-2.

[4] J. Stephen, S. Pappas, Diabetic retinopathy, https://www.center4retina.org/our-services/diabetic-retinopathy.

[5] B. Zhang, X. Wu, J. You, Q. Li, F. Karray, Detection of microaneurysms using multi-scale correlation coefficients, Pattern Recognit. 43 (6) (2010) 2237–2248, https://doi.org/10.1016/j.patcog.2009.12.017.

[6] U.R. Acharya, E.Y.-K. Ng, J.-H. Tan, S.V. Sree, K.-H. Ng, An integrated index for the identification of diabetic retinopathy stages using texture parameters, J. Med. Syst. 36 (3) (2012) 2011–2020, https://doi.org/10.1007/s10916-011-9663-8.

[7] M. Islam, A.V. Dinh, K.A. Wahid, Automated diabetic retinopathy detection using bag of words approach, J. Biomed. Eng. 10 (5) (2017) 86–96, https://doi.org/10.4236/jbise.2017.105B010.

[8] M. Chetoui, M.A. Akhloufi, M. Kardouchi, Diabetic retinopathy detection using machine learning and texture features, in: 2018 IEEE Canadian Conference on Electrical & Computer Engineering, CCECE, IEEE, 2018, pp. 1–4.

[9] N. Gharaibeh, O.M. Al-Hazaimeh, B. Al-Naami, K.M. Nahar, An effective image processing method for detection of diabetic retinopathy diseases from retinal fundus images, Int. J. Signal Imaging Syst. Eng. 11 (4) (2018) 206–216, https://doi.org/10.1504/IJSISE.2018.093825.
[10] A. Colomer, J. Igual, V. Naranjo, Detection of early signs of diabetic retinopathy based on textural and morphological information in fundus images, Sensors 20 (4) (2020) 1005, https://doi.org/10.3390/s20041005.
[11] C. Lam, D. Yi, M. Guo, T. Lindsey, Automated detection of diabetic retinopathy using deep learning, AMIA Jt. Summits. Transl. Sci. Proc. 2018 (2018) 147–155.
[12] S.M.S. Islam, M.M. Hasan, S. Abdullah, Deep learning based early detection and grading of diabetic retinopathy using retinal fundus images, arXiv preprint, arXiv:1812.10595, 2018, https://doi.org/10.48550/arXiv.1812.10595.
[13] Y. Hatanaka, K. Ogohara, W. Sunayama, M. Miyashita, C. Muramatsu, H. Fujita, Automatic microaneurysms detection on retinal images using deep convolution neural network, in: 2018 International Workshop on Advanced Image Technology, IWAIT, IEEE, 2018, pp. 1–2.
[14] Y.-H. Li, N.-N. Yeh, S.-J. Chen, Y.-C. Chung, et al., Computer-assisted diagnosis for diabetic retinopathy based on fundus images using deep convolutional neural network, Mob. Inf. Syst. 2019 (2019), https://doi.org/10.1155/2019/6142839.
[15] N. Eftekhari, H.-R. Pourreza, M. Masoudi, K. Ghiasi-Shirazi, E. Saeedi, Microaneurysm detection in fundus images using a two-step convolutional neural network, Biomed. Eng. Online 18 (1) (2019) 1–16, https://doi.org/10.1186/s12938-019-0675-9.
[16] D.J. Hemanth, O. Deperlioglu, U. Kose, An enhanced diabetic retinopathy detection and classification approach using deep convolutional neural network, Neural Comput. Appl. 32 (3) (2020) 707–721, https://doi.org/10.1007/s00521-018-03974-0.
[17] A. Garifullin, L. Lensu, H. Uusitalo, Deep Bayesian baseline for segmenting diabetic retinopathy lesions: advances and challenges, Comput. Biol. Med. 136 (2021) 104725, https://doi.org/10.1016/j.compbiomed.2021.104725.
[18] Fatima, M. Imran, A. Ullah, M. Arif, R. Noor, A unified technique for entropy enhancement based diabetic retinopathy detection using hybrid neural network, Comput. Biol. Med. 145 (2022) 105424, https://doi.org/10.1016/j.compbiomed.2022.105424.
[19] N. Tsiknakis, D. Theodoropoulos, G. Manikis, E. Ktistakis, O. Boutsora, A. Berto, F. Scarpa, A. Scarpa, D.I. Fotiadis, K. Marias, Deep learning for diabetic retinopathy detection and classification based on fundus images: a review, Comput. Biol. Med. 135 (2021) 104599, https://doi.org/10.1016/j.compbiomed.2021.104599.
[20] R. Vij, S. Arora, A systematic review on diabetic retinopathy detection using deep learning techniques, Arch. Comput. Methods Eng. 30 (3) (2023) 2211–2256, https://doi.org/10.1007/s11831-022-09862-0.
[21] N.B.A. Mustafa, W. Zaki, A. Hussain, J.C. Hamzah, A fully-automated retinal blood vessels detection using filling algorithm, Inf., Int. Interdiscip. J. 20 (1) (2017) 665–673.
[22] Z. Yavuz, C. Köse, Blood vessel extraction in color retinal fundus images with enhancement filtering and unsupervised classification, J. Healthc. Eng. 2017 (2017), https://doi.org/10.1155/2017/4897258.
[23] A. Elbalaoui, M. Fakir, K. Taifi, A. Merbouha, Automatic detection of blood vessel in retinal images, in: 2016 13th International Conference on Computer Graphics, Imaging and Visualization, CGiV, IEEE, 2016, pp. 324–332.
[24] H. Hassan, S.A. Azis, A simple approach of blood vessels detection in retinal images using MATLAB, in: 2012 IEEE Student Conference on Research and Development, SCOReD, IEEE, 2012, pp. 245–249.
[25] W. Zhou, H. Wu, C. Wu, X. Yu, Y. Yi, Automatic optic disc detection in color retinal images by local feature spectrum analysis, Comput. Math. Methods Med. 2018 (2018), https://doi.org/10.1155/2018/1942582.
[26] L.A. Muhammed, Localizing optic disc in retinal image automatically with entropy based algorithm, Int. J. Biomed. Imaging 2018 (2018), https://doi.org/10.1155/2018/2815163.
[27] A.S. Abdullah, Y.E. Özok, J. Rahebi, A novel method for retinal optic disc detection using bat meta-heuristic algorithm, Med. Biol. Eng. Comput. 56 (11) (2018) 2015–2024, https://doi.org/10.1007/s11517-018-1840-1.
[28] H.M. Ünver, Y. Kökver, E. Duman, O.A. Erdem, Statistical edge detection and circular hough transform for optic disk localization, Appl. Sci. 9 (2) (2019) 350, https://doi.org/10.3390/app9020350.
[29] Z. Fan, Y. Rong, X. Cai, J. Lu, W. Li, H. Lin, X. Chen, Optic disk detection in fundus image based on structured learning, IEEE J. Biomed. Health Inform. 22 (1) (2017) 224–234, https://doi.org/10.1109/JBHI.2017.2723678.
[30] S. Sadhukhan, G.K. Ghorai, S. Maiti, G. Sarkar, A.K. Dhara, Optic disc localization in retinal fundus images using faster R-CNN, in: 2018 Fifth International Conference on Emerging Applications of Information Technology, EAIT, IEEE, 2018, pp. 1–4.
[31] D. Niu, P. Xu, C. Wan, J. Cheng, J. Liu, Automatic localization of optic disc based on deep learning in fundus images, in: 2017 IEEE 2nd International Conference on Signal and Image Processing, ICSIP, IEEE, 2017, pp. 208–212.
[32] M.N. Bajwa, M.I. Malik, S.A. Siddiqui, A. Dengel, F. Shafait, W. Neumeier, S. Ahmed, Two-stage framework for optic disc localization and glaucoma classification in retinal fundus images using deep learning, BMC Med. Inform. Decis. Mak. 19 (1) (2019) 1, https://doi.org/10.1186/s12911-019-0842-8.
[33] C. Tomasi, R. Manduchi, Bilateral filtering for gray and color images, in: Sixth International Conference on Computer Vision, IEEE Cat. No. 98CH36271, IEEE, 1998, pp. 839–846.
[34] S. Paris, P. Kornprobst, J. Tumblin, F. Durand, et al., Bilateral filtering: theory and applications, Found. Trends Comput. Graph. Vis. 4 (1) (2009) 1–73.
[35] U. Kuran, E.C. Kuran, Parameter selection for CLAHE using multi-objective cuckoo search algorithm for image contrast enhancement, Intell. Syst. Appl. 12 (2021) 200051, https://doi.org/10.1016/j.iswa.2021.200051.
[36] M.U. Akram, S. Khalid, A. Tariq, M.Y. Javed, Detection of neovascularization in retinal images using multivariate m-mediods based classifier, Comput. Med. Imaging Graph. 37 (5–6) (2013) 346–357, https://doi.org/10.1016/j.compmedimag.2013.06.008.
[37] S.S. Kar, S.P. Maity, Detection of neovascularization in retinal images using mutual information maximization, Comput. Electr. Eng. 62 (2017) 194–208, https://doi.org/10.1016/j.compeleceng.2017.05.012.
[38] H. Huang, H. Ma, H.J. van Triest, Y. Wei, W. Qian, Automatic detection of neovascularization in retinal images using extreme learning machine, Neurocomputing 277 (2018) 218–227, https://doi.org/10.1016/j.neucom.2017.03.093.
[39] S. Yu, D. Xiao, Y. Kanagasingam, Machine learning based automatic neovascularization detection on optic disc region, IEEE J. Biomed. Health Inform. 22 (3) (2017) 886–894, https://doi.org/10.1109/JBHI.2017.2710201.
[40] C. Szegedy, V. Vanhoucke, S. Ioffe, J. Shlens, Z. Wojna, Rethinking the inception architecture for computer vision, in: Proceedings of the IEEE Conference on Computer Vision and Pattern Recognition, 2016, pp. 2818–2826.
[41] DRIVE: digital retinal images for vessel extraction [Online], Available: https://drive.grand-challenge.org/. (Accessed 13 August 2019).
[42] E. Decencière, X. Zhang, G. Cazuguel, B. Lay, B. Cochener, C. Trone, P. Gain, R. Ordonez, P. Massin, A. Erginay, et al., Feedback on a publicly distributed image database: the Messidor database, Image Anal. Stereol. 33 (3) (2014) 231–234, https://doi.org/10.5566/ias.1155.
[43] Diabetic retinopathy detection [Online], Available: https://www.kaggle.com/c/diabetic-retinopathy-detection. (Accessed 30 June 2020).
[44] A. Hoover, V. Kouznetsova, M. Goldbaum, Structured analysis of the retina, https://cecas.clemson.edu/~ahoover/stare/, 2000.
[45] DIARETDB0 – standard diabetic retinopathy database [Online], Available: https://www.it.lut.fi/project/imageret/diaretdb0/index.html. (Accessed 30 June 2020).
[46] E.V. Carrera, A. González, R. Carrera, Automated detection of diabetic retinopathy using SVM, in: 2017 IEEE XXIV International Conference on Electronics, Electrical Engineering and Computing, INTERCON, IEEE, 2017, pp. 1–4.
[47] M.D. Saleh, C. Eswaran, An automated decision-support system for non-proliferative diabetic retinopathy disease based on MAs and HAs detection, Comput. Methods Programs Biomed. 108 (1) (2012) 186–196, https://doi.org/10.1016/j.cmpb.2012.03.004.